Results in Chemistry 2 (2020) 100066

Contents lists available at ScienceDirect

Results in Chemistry

journal homepage: www.elsevier.com/locate/rechem

Diazoalkane decay kinetics from UVA-active protein labelling molecules: Trifluoromethyl phenyl diazirines

Ivan Djordjevic [1], Gautama Wicaksono [1], Ivan Solic, Terry W.J. Steele *

School of Materials Science and Engineering (MSE), Nanyang Technological University (NTU), 639798, Singapore

ARTICLE INFO

Article history:
Received 14 May 2020
Accepted 10 August 2020
Available online xxxx

Keywords:
Diazirine
UVA
^{19}F NMR
ATR-FTIR
Diazoalkane
Photoisomerization

ABSTRACT

Trifluoromethyl phenyl diazirine (TPD) molecules are relatively stable carbene precursors, that readily form carbon covalent bonds with proteins. The stability of the diazoalkane intermediates is unknown, as are the factors which control carbene/diazoalkane ratios. This leads to incomplete carbene insertion onto desired compounds. Herein, stability and decay kinetics of diazoalkanes are evaluated from TPDs with various electron drawing groups, including 3-Phenyl-3-(trifluoromethyl)-3H-diazirine (TPD-H), *p*-benzyl alcohol (TPD-CH_2OH), *p*-4-benzoic acid (TPD-COOH), and *p*-benzyl bromide (TPD-CH_2Br). The spectroscopic analysis before and after UVA activation is performed both in dilute chloroform and neat by ^{19}F NMR and ATR-FTIR, respectively. The increase of diazoalkane concentration after UVA exposure was in the order of: TPD-H > TPD-CH_2Br > TPD-CH_2OH > TPD-COOH. Indirect carbene/diazoalkane ratios ranged from 6: 1 to 3:1. Diazoalkane was relatively stable over the evaluation period of 30 min (post-UVA activation) in all compounds except TPD-CH_2Br, which exhibits an 11 min half-life.

1. Introduction

Photoaffinity labelling and tissue adhesives exploit diazirine's ability of non-specific covalent insertion mediated photoactivation [1–3]. This requires grafting of diazirine groups on macromolecules with reactive functional groups of hydroxyl (–OH), carboxyl (–COOH) or bromide (–Br). Photoreaction products of diazirine include carbene and diazoalkanes that rapidly form covalent bonds to proximate amino acids [4]. As presented in Scheme 1, upon activation with UVA light diazirine molecules (a) either photoisomerize into diazoalkane (b) or transform directly into reactive carbene species (c). The kinetics of diazoalkane-to-carbene conversion is dependent on substituents nearby diazirine and the solvating environment (i.e. solvent polarity) [5,6]. Protein labelling and covalent insertion efficiency is dependent on the conversion kinetics after photoactivation. Exploitation of carbene insertion reactions has evolved new types of voltage- and UVA-activated adhesive formulations [2,7–10]. Both voltage- and UVA-generated carbenes covalently insert into tissue proteins providing new strategies for adhering to wet tissue substrates. For these reasons, the quantitative determination of diazoalkane decay kinetics is necessary for accurate photoaffinity labelling as well as effective tissue proximation by interfacial carbene insertion.

Trifluoromethyl phenyl diazirines (TPDs; Scheme 1) are chemically stable substituents compared to aliphatic diazirines [11–14]. Trifluoromethyl group ($-CF_3$) prevents intramolecular generation of alkenes, favouring the high energy carbene [1,15–18]. Due to the strength of C—F bond, $-CF_3$ group is not prone to structural rearrangements in excited state, leading to a more efficient carbene insertion pathways [19]. The phenyl substituents in aryl-diazirines influence the energy barrier for photolysis and the ratio of carbene/diazoalkane species (Scheme 1) [20]. The aromatic ring enhances the stability of diazoalkane compounds [21], where the diazoalkane isomer concentration can reach 35% [11]. The exact kinetic parameters (i.e. half-life, decay rate constants) of TPD photodecay under known parameters (wavelength, energy dose, stability), compounds are unknown, which adds to complexity of TPD's utilization [22–24].

Depending on the chemistry of diazirine substituents some diazoalkane intermediates have longer lifetimes that should enable quantitative analysis of decay kinetics by FTIR spectroscopy [6,25]. The FTIR analysis can be extended to detect diazoalkane intermediates in both solution (2042 cm^{-1}) and in solid state (2033 cm^{-1}) [26]. Published reports indicate TPD conversion of 20–35% into diazoalkane under 350 nm UVA light (450 W); reported range of diazoalkane half-life is from 18 s to 22 min depending on both the TPD concentration in solvent medium and the functional group/chemical structure on *p*-position within TPD molecule [11,27]. Early investigations of diazoalkane from diazirine photoisomerization exploited IR spectroscopy, but they report no effects of aryl-substituents [28]. To our knowledge, there is no systematic study that quantitatively correlates

* Corresponding author.
E-mail address: wjsteele@ntu.edu.sg (T.W.J. Steele).
[1]Equal contribution as the first authors.

https://doi.org/10.1016/j.rechem.2020.100066

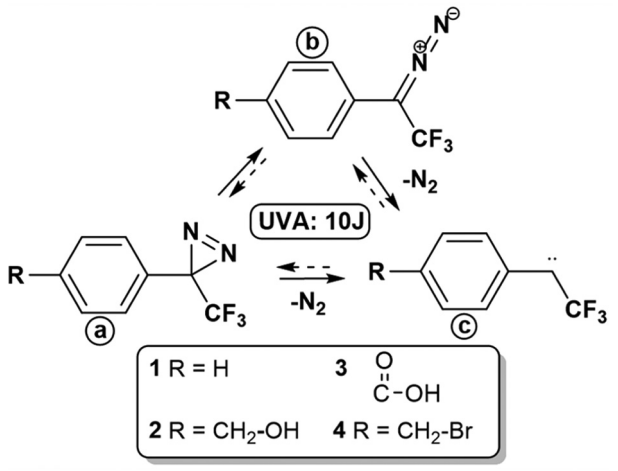

Scheme 1. TPDs (a: **1**–**4**); diazoalkane (b); carbene (c) intermediates generated upon UVA-activation.

diazoalkane decay kinetics to the chemistry of functional group attached to *p*-position on TPD molecules. This is rectified with solvent-free analysis of TPDs presented in Scheme 1: (**1**) 3-Phenyl-3-(trifluoromethyl)-3H-diazirine (TPD-H; unsubstituted TPD used as control), (**2**) 4-[3-(trifluoromethyl)-3H-diazirin-3-yl] benzyl alcohol (TPD-CH_2OH), (**3**) 4-[3-(trifluoromethyl)-3H-diazirin-3-YL] benzoic acid (TPD-COOH) and (**4**) 4-[3-(trifluoromethyl)-3H-diazirin-3-yl] benzyl bromide (TPD-CH_2Br); with FTIR spectroscopy in attenuated total reflectance (ATR) mode. Note that compounds: **1**, **2**, and **4** are liquids and **3** is solid at 25 °C.

Fluorine's presence in TPD compounds enables quantitative analysis by ^{19}F NMR [24] but the reactive carbenes inevitably react with solvent medium, glass surfaces [29], and form intermolecular adducts that precipitate—preventing a thorough NMR-based quantitative analysis of diazoalkane decay kinetics. However, ^{19}F NMR enables detection of diazoalkane intermediate in situ. To the best of our knowledge, this is the first systematic investigation of UVA-activated TPDs by functional groups in *para* position (**1**–**4**; Scheme 1). Furthermore, all the reaction products generated by UVA activation of TPDs (in chloroform) are detected and reported. The major objective of this work is quantitative identification of diazoalkane intermediates and their stability by both ^{19}F NMR (in solvent medium) and ATR-FTIR (solvent-free native state) spectroscopy methods. The work is based on hypotheses that: (i) diazoalkane stability/decay depends on the nature of the medium where TPD compounds are activated with UVA light (i.e. solution used for NMR analysis or exposure to atmosphere when analysed in neat state with ATR-FTIR); (ii) the diazoalkane species in UVA-activated TPDs, chosen for this study, are stable enough to be quantitatively analysed with relatively simple ATR-FTIR probe that requires no sample preparation; (iii) TPDs do not undergo intramolecular rearrangement in reactive state as both phenyl and $-CF_3$ groups will not react with the carbene intermediate. Diazoalkane decay kinetics and four TPD aryl-substituents (**1**–**4**; Scheme 1) are analysed before and after 10 J UVA activation at 365 nm; the diazoalkane FTIR peak absorbance (~2090 cm^{-1}) values are collected and normalized with respect to UVA dose, time, and peak height. First-order kinetics, diazoalkane quantitation, and real-time stability up to 30 min evaluate the nature of TPD molecules in their native and diluted state.

2. Materials and methods

2.1. Materials

Hexafluoro benzene (186.06 $g \cdot mol^{-1}$; HFB), 3-phenyl-3-(trifluoromethyl)-3H-diazirine (186.13 $g \cdot mol^{-1}$; TPD-H; **1**), 4-[3-(trifluoromethyl)-3H-diazirin-3-yl]benzyl alcohol (216.16 $g \cdot mol^{-1}$; TPD-CH_2OH; **2**), and 4-[3-(trifluoromethyl)-3h-diazirin-3-yl]benzyl bromide (279.06 $g \cdot mol^{-1}$; TPD-CH_2Br; **4**) are purchased from TCI Chemicals, Japan. 4-[3-(Trifluoromethyl)-3H-diazirin-3-YL] Benzoic acid (230.14 $g \cdot mol^{-1}$ TPD-COOH; **3**) is synthesized from TPD-CH_2OH in the following procedure. A solution of TPD-CH_2OH (1 mol. eq.) and potassium hydroxide (1.55 mol. eq.; 0.6 M KOH solution) is dissolved in a mixture of water/dioxane (5/1), cooled down to 0 °C in an ice bath and potassium permanganate (1.5 eq.) is added portion-wise. The biphasic reaction mixture is vigorously stirred at room temperature overnight (18 h). The suspension is filtered through a pad of Celite®. The filtrate is cooled in an ice bath and acidified with 2 M HCl to pH = 1. The obtained white precipitate is filtered off and dissolved in ethanol. The organic layer is washed 5 times with water and one time with brine, dried with anhydrous $MgSO_4$, and the solvent is evaporated in vacuum to yield pure TPD-COOH as a pale-yellow solid (yield: 92%). ^1H NMR (400 MHz, $CDCl_3$) δ (ppm): 8.14 (d, J = 8.4 Hz, 2H), 7.29 (d, J = 8.4 Hz, 2H). ^{19}F NMR (400 MHz, $CDCl_3$) δ (ppm):−64.7 (s).

2.2. NMR spectroscopy analysis of TPD compounds before and after UVA activation

TPDs are analysed with NMR (JEOL ECA 400) at 400 MHz with $CDCl_3$ used as a solvent. Both ^{19}F and ^1H NMR spectra before and after UVA activation are collected and analysed. The TPD samples are dissolved and mixed with HFB (internal standard) and subsequently UVA-activated with UVA LED Thorlabs SOLIS 365C of dominant wavelength at 365 nm: constant UVA intensity of 100 $mW \cdot cm^{-2}$ is applied over 100 s duration for a total dose of 10 J. All the samples are mixed thoroughly before placing the tube inside the NMR chamber. The spectra are collected for TPDs in the following states: (i) before UVA; (ii) immediately after UVA activation; and (iii) 30 min after UVA activation.

2.3. ATR-FTIR analysis of diazoalkane decay from solvent-free TPD molecules

FTIR spectroscopy is performed using PerkinElmer Frontier IR equipped with attenuated total reflection (ATR) sampling accessory. Pure liquid TPD compounds (**1**, **2** and **4**) are pipetted onto glass slides, while solid powder TPD (**3**) sample is placed between two glass slides of approximate distance 50 μm. TPD samples are UVA-activated with UVA LED Thorlabs SOLIS 365C of dominant wavelength at 365 nm: constant UVA intensity of 100 $mW \cdot cm^{-2}$ is applied over 100 s duration for a total dose of 10 J. The surface of UVA-activated samples is directly placed onto ATR crystal. FTIR spectra are recorded over accumulation of 8 scans at resolution 4 cm^{-1}, at range of 4000 cm^{-1} to 600 cm^{-1}. Spectra are collected on every 1 min for a total of 30 min post-UVA activation. Diazoalkane absorbance values (~2090 cm^{-1}) for all TPD compounds are collected in triplicates and the average absorbances are plotted against time. All the spectra are compared (neat/UVA-activated) and curve-fitted to first order decay equation in OriginPro 2016 software.

3. Results

3.1. ^{19}F NMR analysis of TPD compounds

TPD molecules are deliberately chosen as diazirine precursors due to the stabilizing effect of the aromatic ring and electron-withdrawing $-CF_3$ group [6]. Alkyl-diazirines are not included due to their propensity for intramolecular side reactions [11]. TPD compounds with 'handles' (functional groups on *para* positions) are chosen with respect to those utilized in biochemical conjugation, such as Michael addition of TPD–CH_2Br onto pendant $-NH_2$ groups [9] or ester conjugation of diazirines with either –COOH or –OH [16]. The formation and stability of intermediates generated from TPDs with 3 different functional groups (Scheme

1) is compared to TPD-H, as control. ^{19}F NMR results of TPDs (**1**–**4**; referred to as *dilute* further in text) in Fig. 1A–D (left column) indicate a singlet diazirine peak at −65 ppm and no presence of diazoalkane intermediate that is normally positioned at −56 to −59 ppm [30] (^{1}H NMR spectra and peak assignment with exact values of chemical shifts are presented in Supplementary information; Fig. S1). All ^{19}F NMR signals are referenced to 0.1% hexafluorobenzene ($\delta = -161.6$ ppm, internal standard) [31]. Spectrum of dilute **1** shows the ~5% of azine adduct (judging from the integral values at −67.1 ppm Fig. 1A; left) and TPD **2** shows a doublet peak at −76.4 ppm (inset; Fig. 1B; left) assigned to ether adduct as a results of carbene insertion into –OH group of **2** [30]. Carbenes are known to react readily with alcohols by –OH insertion [22] and the detection of ether dimer (or oligomer) is likely a consequence of exposure of **2** to ambient light [24]. Similar adduct is observed for TPD **3** where the ester peak is detected at −75.9 ppm. TPD **4** displays the diazirine peak without any adducts (Fig. 1C, D; left).

TPD solutions in $CDCl_3$ (within 5 mm NMR tubes) are irradiated at 10 J UVA and vortexed prior to NMR analysis. ^{19}F NMR spectra of UVA activated **1**–**4** recorded within 10 min (Fig. 1A–D; right) show reduction of diazirine peak integral and the appearance of diazolkane at −57.2 to −57.3 ppm; the ^{19}F NMR spectra of TPDs 30 min after UVA (not shown) had no change in chemical shifts (Fig. 1A–D; right). Apart from diazoalkane and diazirine peaks (still persistent 30 min after UVA activation) there are other trifluoro phenyl molecular species such: azines,

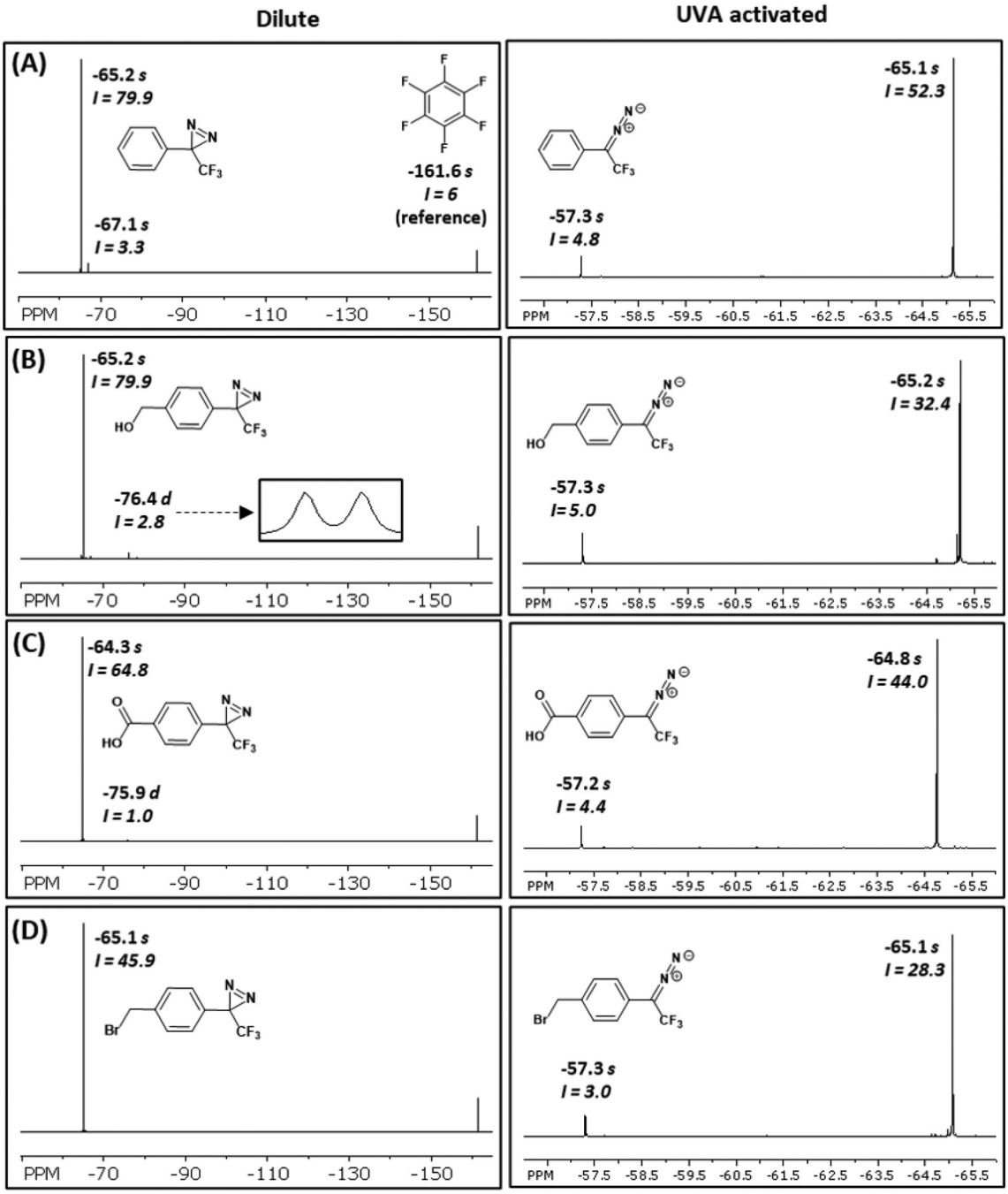

Fig. 1. ^{19}F NMR spectra of dilute (left column) and UVA-activated (10 J; right column) TPDs with chemical shifts (δ_{ppm}) for diazirine (−65 ppm) and diazoalkanes (−57 ppm); corresponding peak integrals (*I*) calculated by taking HFB peak as reference are shown in each spectrum: (A) **1** TPD-H; (B) **2** TPD-CH_2OH; (C) **3** TPD-COOH; (D) **4** TPD-CH_2Br.

Table 1
Calculated concentration changes measured with ^{19}F NMR of TPD (**1**–**4**) diazoalkane[a] and diazirine[b] peaks normalized to dilute compounds and expressed in percentages for UVA activated TPDs and for TPDs 30 min upon UVA (10 J)[c].

NMR shifts (ppm)	Functional group	**1** (%)		**2** (%)		**3** (%)		**4** (%)	
		UVA	30 min	UVA	30 min	UVA	30 min	UVA	30 min
−57.2/−57.3	Diazoalkane	100	97.8	100	95.6	100	97.5	100	80.0
−65.1/−65.2	Diazirine	65.7	65.2	40.6	40.4	67.9	69.5	61.7	56.3

[a] Diazoalkane decay (%) = $([DA]^{30min}/[DA]^{UVA}) \times 100$; $[DA]^{30min}$ is concentration of diazoalkane measured 30 min upon UVA activation; $[DA]^{UVA}$ is concentration of diazoalkane measured immediately after UVA activation.
[b] Diazirine decay (%) immediately after UVA = $([DZ]^{UVA}/[DZ]^{neat}) \times 100$; Diazirine decay (%) 30 min after UVA = $([DZ]^{30min}/[DZ]^{neat}) \times 100$; $[DZ]^{UVA}$, $[DZ]^{neat}$ and $[DZ]^{30min}$ are diazirine concentrations measured immediately after UVA activation, dilute compound and 30 min after UVA activation respectively.
[c] The calculated concentration values from ^{19}F NMR integration are shown in Supplementary information, Table S1.

ketones, alcohols, chlorides, ethers and esters. The full account on the identification, peak assignment, and concentration of TPDs detected in ^{19}F NMR spectra for: dilute, UVA activated, and 30 min post-activation samples are presented in Supplementary information (Fig. S2; Table S1).

Overall TPD concentration after UVA exposure drops by 20%, 35%, 20% and 25% for **1**, **2**, **3** and **4**, respectively (Table S1). This concentration reduction is a result of either precipitation (not visually observed) or carbene insertion onto Si-OH of glass NMR tubes [29]. TPDs form stable diazoalkanes in the range of 6.1–6.8% as a result of conversion from diazirine under the given parameters (Table S1). Results in Table 1 show the stability of remained diazirine 30 min after exposure to UVA light where the highest rate of diazirine decay (−5.4%) is recorded for **4** while diazirine groups of **1** and **2** decay is <1%. Increase in diazirine ^{19}F NMR peak for +1.6% is recorded for TPD **3** and is attributed to experimental error, reverse photoisomerization, or both. Regarding the diazoalkane decay Table 1 displays the persistence/stability in the order of: **1** > **3** > **2** > **4**; diazoalkane peak integral of **1** decreases only for −2.2% while the same peak (−57.2 ppm) of **4** decreases for −20.0% within 30 min upon UVA activation.

There is a clear correlation between carbene/diazoalkane ratios and *para* substituents that can be exploited (Table S2). Electron-donating groups promote carbene formation (**2**, carbene ratio/diazoalkane = 6:1) while electron-withdrawing groups (**3**) show lower carbene/diazoalkane ratio = 3:1. Weak electron-donating groups show moderate carbene/diazoalkane ratio = 4:1 in a case of **1** and **4** (Table S2). The electronic effect of *para* substituent on the rate of chemical reactions in general is determined by Hammett substituent constant.

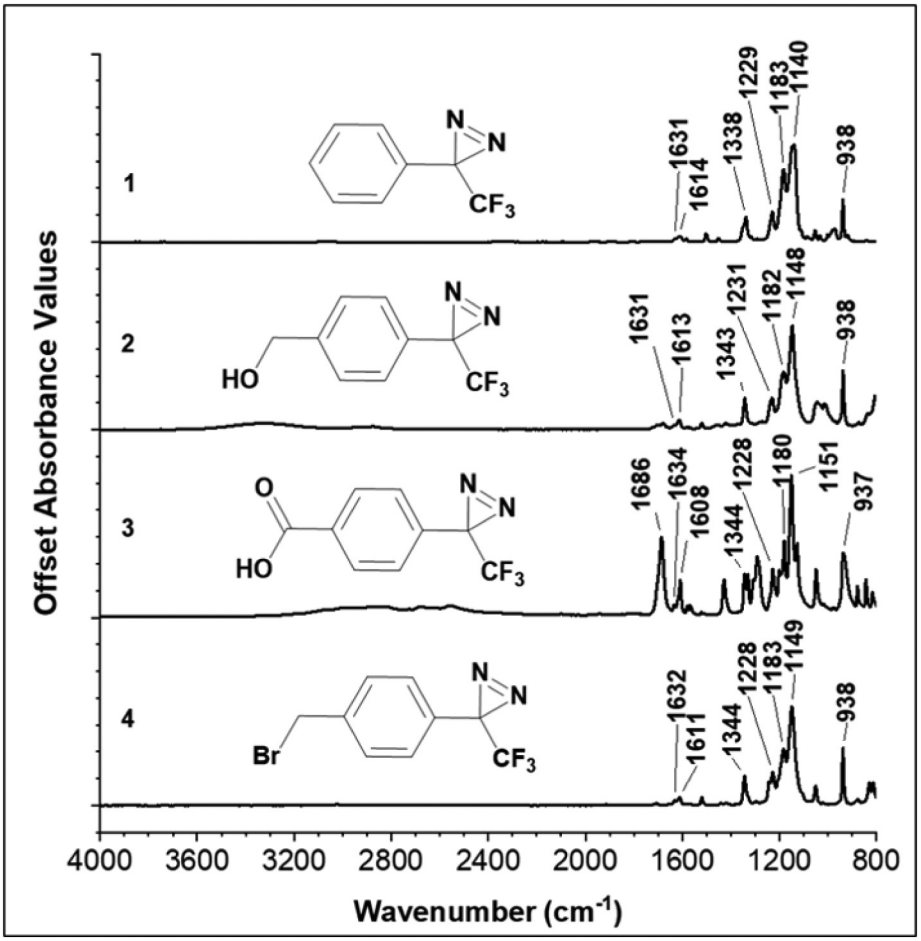

Fig. 2. FTIR spectra of neat TPDs (**1**–**4**).

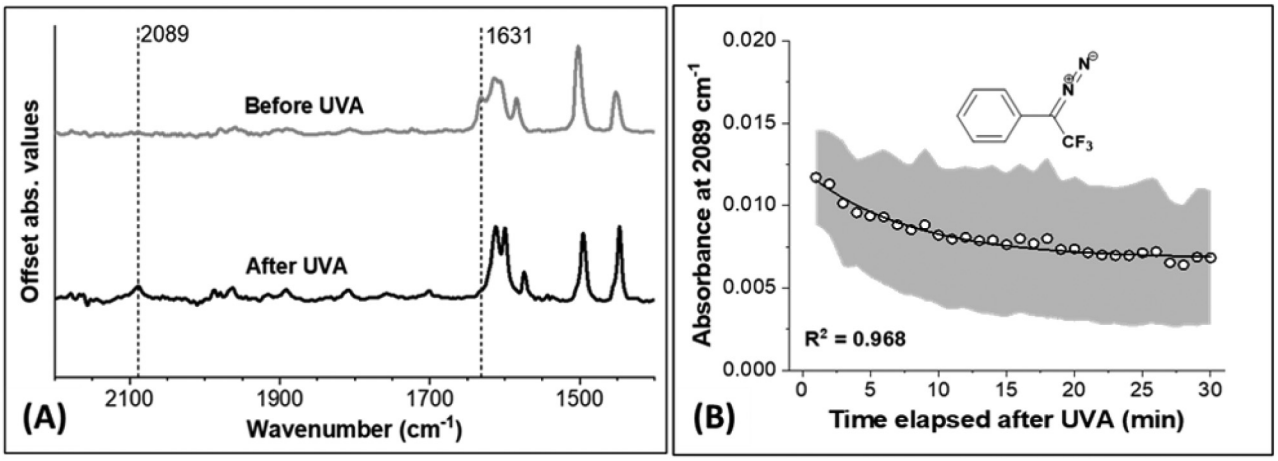

Fig. 3. Diazoalkane detection and decay kinetics of TPD-H (**1**): (A) FTIR spectrum before (top) and after UVA exposure at 10 J (bottom); (B) absorbance readings at peak 2089 cm^{-1} vs time post-UVA activation (standard deviation range is indicated in grey; n = 3).

Decrease of carbene/diazoalkane ratio: **2** > **4** > **3** correlates to values of Hammett constants: 0.11, 0.14 and 0.45 for **2**, **4** and **3** respectively (Hammett constant = 0 for reference compound TPD-H) [32]. Note that above interpreted results are limited to TPDs under dissolved condition in deuterated chloroform.

3.2. Solvent-free ATR-FTIR analysis: diazoalkane decay kinetics profile of TPD compounds

Solvent-free TPDs are analysed with ATR-FTIR spectroscopy and the measured spectral region for **1**–**4** is presented in Fig. 2. Similar to other trifluoromethyl-phenyl compounds (i.e. trifluoromethyl benzoic acid) the $-CF_3$ group of analysed TPDs shows strong band from symmetric stretching at ~1140 cm^{-1} region [33]. The diazirine ring itself is expected to be found near 1630 cm^{-1}, but this symmetric band is weak. Peak at 1631 cm^{-1} is assigned to N═N [34] while 1610 cm^{-1} and 1344 cm^{-1} are assigned to the C—N bond. The distinctive peak at 938 cm^{-1} originates from out-of-plane bending vibrations of phenyl ring, and exploited as a peak height reference [35]. TPD **2** shows broad –OH peak centred at 3400 cm^{-1}; –OH peak from –COOH group of **2** is in the region of 2200–3200 cm^{-1} along with the strong characteristic carbonyl peak at 1686 cm^{-1}. Spectrum of **4** aligns with **1** because —Br peak is normally found below 600 cm^{-1} which is outside of the measurement range.

Liquid TPD compounds are activated with a total dose of 10 $J \cdot cm^{-2}$ in order to avoid thermal activation they may occur under prolonged exposure (10 MJ under Hg lamp) [36]. FTIR spectra are collected from the sample surface within 5 min after UVA activation and are normalized for comparison (Figs. 3A–6A). Real-time FTIR analysis observes diazoalkane decay after irradiation. Diazoalkane decay is then evaluated for first order kinetics up to 30 min (Figs. 3B–6B) [17]. Raw datasets (n = 3) are shown in Supplementary information (Fig. S3).

The relative change of absorbance assigned to diazirine (N=N; 1630 cm^{-1}) is also recorded, by the weak signal that will come with a high degree of error due to stronger neighbouring peaks. Numerical values of both peaks (diazirine and diazoalkane) along with C—N stretching vibration (1130 cm^{-1}) before and after UVA activation are displayed in Tables 2 and 3 respectively. Major absorbance peaks are normalized against the aromatic C—H (937–967 cm^{-1}; Tables 2 and 3) [35] and $-CF_3$ as an alternative (Tables S3 and S4) [34]. Exact values of absorbances are listed in Fig. S4. Upon UVA exposure, all samples display the reduction of diazirine absorbance at 1630 cm^{-1}, and there is an obvious appearance of 2090 cm^{-1} broad peak assigned to diazoalkane (Figs. 3–6A; Tables 2 and 3) [37]. This is consistent with expected carbene vs diazoalkane formation; carbene is not detected in FTIR because of its nanosecond lifetime [20].

No diazoalkane peaks are observed in dilute TPDs by ^{19}F NMR (Fig. 1), but ATR-FTIR detects weak peaks at 2090 cm^{-1} (Fig. S4) for neat **2**–**4**. Absorbance values after UVA activation are presented in Table 3. TPDs **1** and **4** show diazirine decay (1630 cm^{-1}; Table 3) while **2** and **3** show an increase of 1.5% and 19.1% (respectively) after UVA activation. Diazirine peak overlaps with C—N peak at 1610 cm^{-1} that is also subject to transformation during the activation with UVA light. The peak overlap accounts for the observed increase.

The lowest absorbance value at 2090 cm^{-1} is recorded for **1** (Fig. 3A; Table 3) and a 32% decay over 30 min is shown in Fig. 3B. TPD **2** has the strongest diazoalkane peak (Fig. 4A; Table 3; Fig. S3). The diazoalkane absorbance value of **2** drops only 1.9% after 30 min as displayed in Fig. 4B. The absorbance of broad –OH peak (3300 cm^{-1}) decreased by 11% (Fig. S5A) after absorbing UVA light. This is attributed to carbene insertion onto *para*-positioned $-CH_2-$**OH** [22]. Although compound **3**

Table 2
FTIR absorbance values of neat **1**–**4** TPDs.

FTIR peak cm^{-1}	Functional group	Onset absorbance values				Normalized absorbance ratio w.r.t. phenyl peak[a]			
		1	**2**	**3**	**4**	**1**	**2**	**3**	**4**
2090–2098	Diazoalkane	0	0.0028	0.0267	0.0010	0	0.0064	0.0556	0.0023
1630–1634	Diazirine	0.0241	0.0349	0.0981	0.0380	0.0766	0.0793	0.2043	0.0887
1338–1344	C-N	0.1851	0.2337	0.3255	0.2190	0.5885	0.5316	0.6778	0.5114
1125–1151	CF_3	0.7247	0.7726	1.06	0.7361	2.3043	1.7575	2.2074	1.7191
937–967	Phenyl	0.3145	0.4396	0.4802	0.4282	1	1	1	1

[a] Normalized absorbance ratio ($A^{1/norm}_{diazirine}$) for compound **1** = $A^{1}_{diazirine}/A^{1}_{phenyl}$ = 0.0241/0.3145 = 0.0766.

Table 3
FTIR spectra of UVA-activated **1**–**4** TPDs immediately after UVA exposure; % indicate increase/decrease (+/−) in normalized ratios calculated* against untreated TPDs (outlined in Table 2).

FTIR peak cm^{-1}	Functional group	Onset absorbance values				Normalized absorbance ratio, w.r.t. phenyl peak*			
		1	**2**	**3**	**4**	**1**	**2**	**3**	**4**
2090–2095	Diazoalkane[a]	0.0147	0.0823	0.0417	0.0397	0.0335 (+100%)	0.2140 (+97.0%)	0.1883 (+76.1%)	0.1025 (+97.7%)
1630–1634	Diazirine[b]	0.0127	0.0310	0.0539	0.0176	0.0290 (−62.1%)	0.0806 (+1.5%)	0.2433 (+19.1%)	0.0454 (−48.8%)
1339–1343	C-N[c]	0.1981	0.2342	0.1066	0.0965	0.4520 (−23.2%)	0.6091 (+14.6%)	0.4813 (−29.0%)	0.2491 (−51.3%)
1121–1151	CF_3	0.6430	0.6130	0.3946	0.6946	1.4670	1.5943	1.7815	1.7930
937–967	Phenyl	0.4383	0.3845	0.2215	0.3874	1	1	1	1

[a] Diazoalkane concentration change (%) for **2** $= [(A_{diazo}^{2/norm\ UVA} - A_{diazo}^{2/norm\ Neat}) / A_{diazo}^{2/norm\ UVA}] \times 100 = [(0.214 - 0.0064) / 0.214] \times 100 = 97.0\%$.
[b] Diazirine concentration change (%) for **4** $= [(A_{diazirine}^{4/norm\ UVA} - A_{diazirine}^{4/norm\ Neat}) / A_{diazirine}^{4/norm\ Neat}] \times 100 = [(0.0454 - 0.0887) / 0.0887] \times 100 = -48.8\%$.
[c] Change in concentration of C—N bonds (%) for **3** $= [(A_{C-N}^{3/norm\ UVA} - A_{C-N}^{3/norm\ Neat}) / A_{C-N}^{3/norm\ Neat}] \times 100 = [(0.4813 - 0.6778) / 0.6778] \times 100 = -29.0\%$.

shows intermediate concentration of diazoalkane within minutes after absorbing UVA dose (Table 3), Fig. 5A indicates reduction of carbonyl peak at 1686 cm^{-1}. Similar to **2**, compound **3** results in more pronounced reduction of carboxyl –OH group as the UVA activation caused a decrease in absorbance of characteristic broad peak at 2200–3200 cm^{-1} [38] down to 37.9% in comparison to neat **3** as a consequence of carbene insertion (Fig. S5B). This result is in line with ^{19}F NMR analysis where both ether and ester bonds (for **2** and **3** respectively) are detected (Fig. S2; Table S1). The concentration of diazoalkane from **3** first increases within 5 min post-UVA and later results with only 0.7% of diazoalkane decay after 30 min (Fig. 5B). TPD **4** has a relatively smaller diazoalkane concentration in comparison to **3** (Fig. 6A; Table 3), however Fig. 6B shows diazoalkane decay of 57.6% after 30 min. FTIR spectrum of **4** (Fig. 6A) reveals a new peak at 1719 cm^{-1} characteristic to >C=O from ketone group [39]. The hypothesized explanation is that bromomethyl undergoes autoxidation sequence. Primary carbon radical forms a peroxide bridge that yields two benzaldehyde equivalents under photooxidation [40]. Benzaldehyde reacts exothermically with diazoalkane, forming the ketone (1716 cm^{-1} peak) as predicted by the Büchner–Curtius–Schlotterbeck reaction [41]. Ketone by-product is also identified with ^{19}F NMR (Fig. S2) in all UVA-activated TPDs with the highest concentration of trifluoromethyl phenyl ketone (−71.3 to −71.6 ppm) detected for TPD-CH_2Br (Table S1).

In summary, from the highest to the lowest diazoalkane formation, analysed TPD compounds follow the order of **1** > **4** > **2** > **3** judging from the absorbance increase at 2090 cm^{-1} measured immediately after exposure to UVA (Fig. S4; Table 3). Over the course of 30 min post-UVA activation, the IR absorbance peaks are still detected with the decrease of diazoalkane absorbance values of: −2.0%, −2.1%, −32.7% and −71.1% for **3**, **2**, **1** and **4** respectively (Figs. 3–6). This result proportionally represents relative diazoalkane persistence/stability in the order of **3** > **2** > **1** > **4**. As there are no solvents present in these compounds during the experiment, this persistence of diazoalkane indicates that as long as there are no reaction sites in reaction proximity (i.e. solutions/mixtures) diazoalkanes from TPDs may remain stable for past 30 min. The data in Figs. 3–6B are fitted according to the first order exponential decay equation $ABS(t) = ABS_0 + ABS_{30} * \exp(-t / \tau) +$ and the values are shown in Table S5. Compounds **1**, **2**, **3** show relatively weak correlation towards the first order exponential decay with $R < 0.99$. Compound **4** shows strong correlation with exponential decay ($R^2 = 0.99$, Fig. 6B) with a half-life of 11 min and rate constant (k) of 0.00103 s^{-1}.

4. Discussion

Diazoalkane formation and decay has been quantified as a function of TPD *para*-substituents with biochemical 'handle' applicability; –CH_2OH (**2**), –COOH (**3**) and – CH_2Br (**4**). ^{19}F NMR analysis exploited the –CF_3 functional group and provided quantitative insight into the various reaction products of intermolecular reactions and carbene/diazoalkane ratios initiated by a 10 J of UVA light. TPD evaluation by ATR-FTIR spectroscopy allowed rapid preparation and real-time recording of diazoalkane decay within a *neat* environment that avoids solvent/carbene cross-reactions. Both spectroscopic methods show that TPD-generated diazoalkanes have relatively long half-lives. This opens prospects for diazoalkane generation on-demand under relatively low UVA intensities, although this is limited to the TPD scaffolds. In situ formation of diazoalkanes is a sought-after technique to avoid the hazardous risks of its synthesis and storage [42]. A method is also presented to calculate the ratios of carbene/diazoalkane through indirect means, with the ratios spanning from 6:1 to 3:1. Presented straightforward ratio calculation is possible with simple benchtop NMR instruments and doesn't require ultrafast spectroscopy or carbon allotrope additives that may

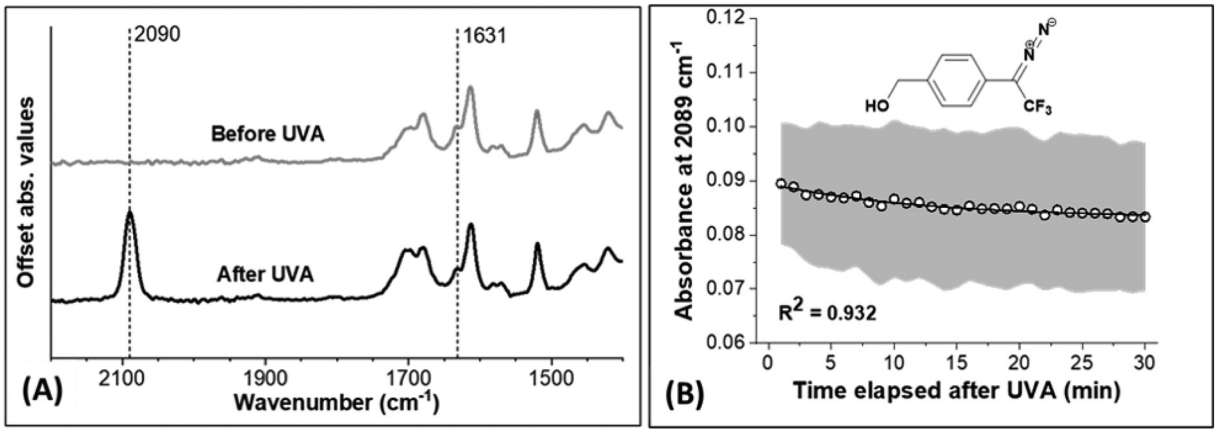

Fig. 4. Diazoalkane detection and decay kinetics of TPD-CH_2OH (**2**): (A) FTIR spectrum before (top) and after UVA exposure at 10 J (bottom); (B) absorbance readings at peak 2090 cm^{-1} vs time post-UVA activation (standard deviation range is indicated in grey; n = 3).

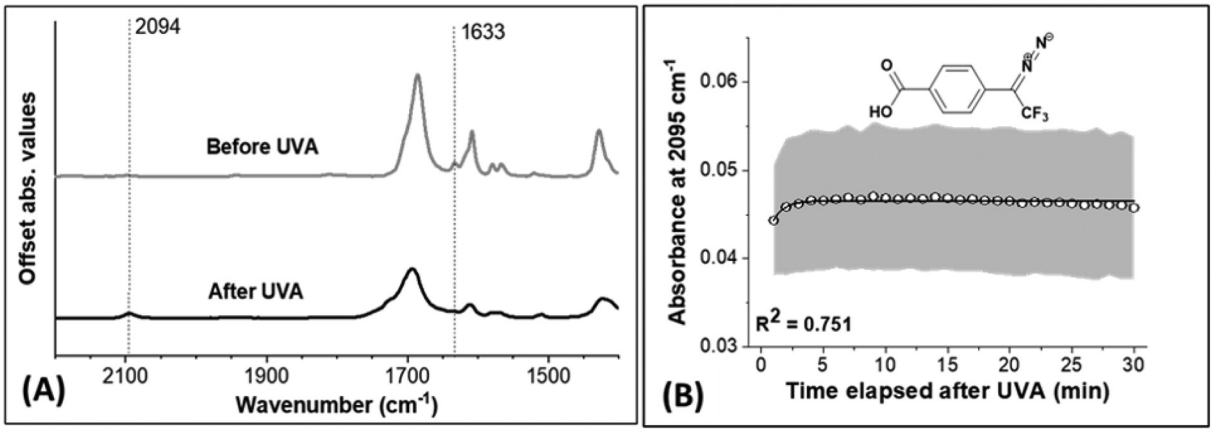

Fig. 5. Diazoalkane detection and decay kinetics of TPD-COOH (**3**): (A) FTIR spectrum before (top) and after UVA exposure at 10 J (bottom); (B) absorbance readings at peak 2095 cm^{-1} vs time post-UVA activation (standard deviation range is indicated in grey; n = 3).

alter the reactive environment [23,43]. In terms of diazoalkane decay, only TPD-CH_2Br demonstrated repeatable first order decay with formation of FTIR peaks attributed to ketones. We speculate diazoalkane is reacting with autooxidation products reminiscent of Büchner–Curtius–Schlotterbeck reactions, known to form ketones [41]. Other TPD-diazoalkanes had weak correlations with respect to first order decay kinetics and were otherwise stable over the 0.5 h evaluation period.

Towards photoaffinity labelling, the results herein display how ^{19}F NMR or solid state FTIR spectroscopy could optimize specific labelling of amino acids (Glu, Asp) by diazoalkane or non-specific labelling through carbene [3]. TPD-COOH had the highest efficiency of diazoalkane formed and would be predicted to give the highest ratio of specific labelling to nucleophilic amino acids of Glu, Asp, and Lys. TPD-CH_2OH had the highest efficiency of carbenes, would be predicted to give the highest ratio of non-specific labelling through C—H, O—H, N—H, and S—H insertion mechanisms. However, carbene/diazoalkane ratios are likely to depend on many factors within the chemical environment. Ratios and efficiency are important in other contexts as well, including cyclopropenation of alkynes where the use of diazoalkanes eliminates catalysis with precious metals [44]. Our paper reports that once generated, the TPD-diazoalkanes decay only 2.5% over the period of 30 min under ambient conditions for selected groups in *para*-position of TPDs.

Three out of the four TPDs merit further studies for further investigation of polymerization. TPD-CH_2OH and TPD-COOH observed an instantaneous drop (11% and 38%, respectively) in the nucleophilic *para*-substituents, suggesting UVA dose may correlate with the degree of polymerization. ^{19}F NMR analysis also confirmed formation of ether and ester bonds (for TPD-CH_2OH and TPD-COOH respectively) which support applications where intermolecular reactions by carbene insertion are needed. Simultaneous photooxidation (-CH_2Br to -aldehyde) and photoisomerization in TPD-CH_2Br may be a promising new route for polyketones. Further mass spectrometry analysis is recommended in order to determine the size and number of ether/ester crosslinking points. Previous investigations of oligomeric diazirines required relatively large light doses of 10 MJ in perfluorinated solvents [36]. In contrast, the 10 J dose chosen herein is more in line with UVA energy used to crosslink diazirine-grafted surgical adhesives and to avoid tissue damage [2,3].

With the inherent TPD properties of cross-linking amino acids and monomer polymerization, stimuli-responsive biomaterials are underway. Grafting TPDs onto biocompatible polymers is an emerging bioadhesives strategy to overcome limitations with acrylates and two-part adhesives [3,45–47]. In this tissue adhesive platform, diazirine end-groups covalently anchor onto tissues upon voltage or UVA activation of 10–20 J and therefore enable tissue proximation in surgical procedures. Voltage activation differs from photocuring, as no diazoalkane intermediates are observed (similar to thermocuring) [48]. Simultaneously, carbene-inserted crosslinked polymer matrix provides elastomeric layer that is biomechanically compatible with tissue interfaces [3,49]. This emerging strategy may benefit from the presence of diazoalkane, in terms of extended times for surgical interventions. The

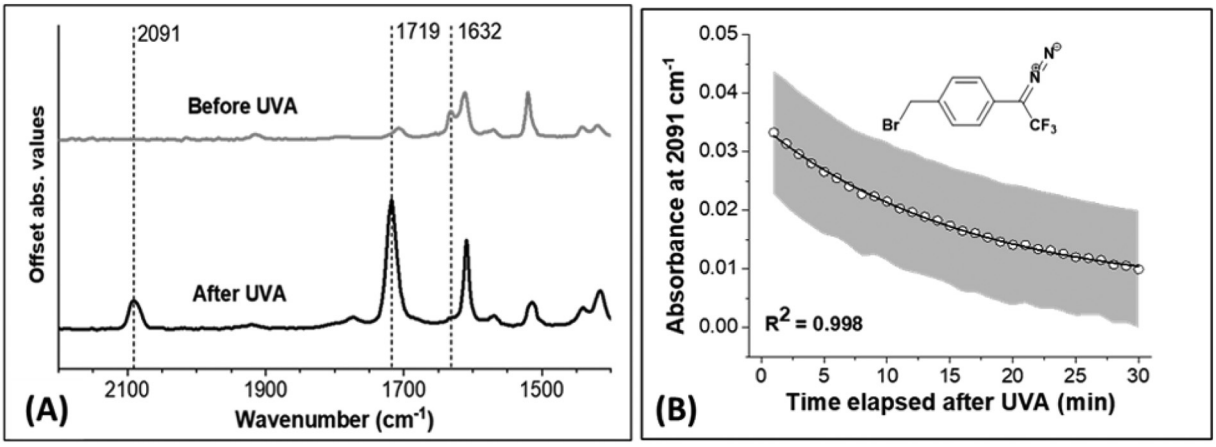

Fig. 6. Diazoalkane detection and decay kinetics of TPD-CH_2Br (**4**): (A) FTIR spectrum before (top) and after UVA exposure at 10 J (bottom); (B) absorbance readings at peak 2091 cm^{-1} vs time post-UVA activation (standard deviation range is indicated in grey; n = 3).

extended half-life of diazoalkane may be leveraged for alternative designs.

Pendant side groups are one of many factors that can shift the photolysis of diazirine and generation of diazoalkane. Generally, the position of diazoalkane band is correlated to the density of hydrogen bond donor [50]. The detection of diazoalkane peak wavenumbers are different from several previous studies and those are in the range of 2020–2135 cm^{-1} [17]. Care should be taken to distinguish diazonium salts (characteristic band between 2245 and 2280 cm^{-1} [51–53]) from diazoalkane that in some cases could exist in equilibrium. Diazo-to-diazonium equilibrium generally occurs in protic solvents [4] unlike the experimental conditions reported in this paper (*neat* and *dilute* TPDs). TPDs have shown a narrow range for diazoalkane (2090–2098 cm^{-1}) with persistence that varies from 2% up to 71% decay over the period of 30 min. Regarding the potential presence of diazonium species, it should be noted that the highest shift from 2090 cm^1 absorbance towards diazonium resonance was recorded for TPD-COOH at 2095 cm^{-1}. Another important conclusion is the noted absence of peaks characteristic to toxic species such as hydrofluoric acid (HF, −198 ppm) [54] or fluoroform ($CHCF_3$, −79.5 ppm) [55]. This is particularly important for diazirine-grafted macromolecular surgical adhesives [3].

5. Conclusion

Aryl-diazirines with three grafting handles in *para* position were analysed for formation and decay kinetics of the diazoalkane intermediate generated by UVA activation. Both NMR (solution) and ATR-FTIR (neat) spectroscopy analysis of aryl-diazirines revealed that decay kinetics of UVA-generated diazoalkane intermediates and their stability depend on the nature of chemical substituents within diazirine molecules as well as the chemical environment in which diazirine activation occurs: solution and neat compounds. For the first time we report the stability and conversion efficiency of diazoalkane intermediates in neat and diluted states. Quantitative determination of various diazoalkanes gives insight into their ambient stability towards photoaffinity labelling, organic synthesis, and bioadhesive applications.

CRediT authorship contribution statement

Ivan Djordjevic: Writing - original draft, Writing - review & editing, Conceptualization, Methodology, Visualization. **Gautama Wicaksono:** Writing - original draft, Methodology, Formal analysis, Investigation, Data curation, Visualization. **Ivan Solic:** Formal analysis, Investigation, Data curation. **Terry W. J. Steele:** Supervision, Conceptualization, Project administration, Funding acquisition, Writing - review & editing, Visualization.

Declaration of competing interest

Terry W.J. Steele and Ivan Djordjevic are co-inventors of patent application: Hygroscopic, Crosslinking Coatings and Bioadhesives; PCT/SG2018/050452. Authors declare no competing interests.

Acknowledgements

Ministry of Education – Singapore Tier 1 Grant RG17/18 (S): Novel light activated, diazo protecting groups, Ministry of Education - Singapore Tier 2 Grant (MOE2018-T2-2-114): CaproGlu, Double sided wet-tissue adhesives and NTUitive POC (Gap) Fund NGF/2018/05: Aesthetic Applications of CaproGlu Bioadhesives.

Appendix A. Supplementary data

Supplementary data to this article can be found online at https://doi.org/10.1016/j.rechem.2020.100066.

References

[1] L. Dubinsky, B.P. Krom, M.M. Meijler, Diazirine based photoaffinity labeling, Bioorg. Med. Chem. 20 (2) (2012) 554–570.
[2] F. Gao, D. Ivan, M. Vishal, O.R. Richard, P. Oleksandr, S.T.W. J, Elastic light tunable tissue adhesive dendrimers, Macromolecular Bioscience 16 (7) (2016) 1072–1082.
[3] I. Djordjevic, O. Pokholenko, A.H. Shah, G. Wicaksono, L. Blancafort, J.V. Hanna, S.J. Page, H.S. Nanda, C.B. Ong, S.R. Chung, A.Y. Hui Chin, D. McGrouther, J.S. Teo, L.S. Lee, T.W.J. Steele, CaproGlu: multifunctional tissue adhesive platform, Biomaterials 120215 (2020).
[4] N. Kanoh, Photo-cross-linked small-molecule affinity matrix as a tool for target identification of bioactive small molecules, Nat. Prod. Rep. 33 (5) (2016) 709–718.
[5] X. Wang, X. Wang, J. Wang, Application of carbene chemistry in the synthesis of organofluorine compounds, Tetrahedron 75 (8) (2019) 949–964.
[6] D.L.S. Brahms, W.P. Dailey, Fluorinated carbenes, Chem. Rev. 96 (5) (1996) 1585–1632.
[7] L. Gan, N.C. Tan, A. Gupta, M. Singh, O. Pokholenko, A. Ghosh, Z. Zhang, S. Li, T.W. Steele, Self curing and voltage activated catechol adhesives, Chem. Commun. 55 (68) (2019) 10076–10079.
[8] M. Singh, R.D. Webster, T.W.J. Steele, Voltaglue electroceutical adhesive patches for localized voltage stimulation, ACS Appl. Bio Mater. 2 (6) (2019) 2633–2642.
[9] J. Ping, F. Gao, J.L. Chen, R.D. Webster, T.W.J. Steele, Adhesive curing through low-voltage activation, Nat. Commun. 6 (2015) 8050.
[10] R.D. O'Rorke, O. Pokholenko, F. Gao, T. Cheng, A. Shah, V. Mogal, T.W.J. Steele, Addressing unmet clinical needs with UV bioadhesives, Biomacromolecules 18 (3) (2017) 674–682.
[11] J. Brunner, H. Senn, F.M. Richards, 3-Trifluoromethyl-3-phenyldiazirine. A new carbene generating group for photolabeling reagents, J. Biol. Chem. 255 (8) (1980) 3313–3318.
[12] D.M. Dankbar, G. Gauglitz, A study on photolinkers used for biomolecule attachment to polymer surfaces, Anal. Bioanal. Chem. 386 (7–8) (2006) 1967–1974.
[13] M.S. Platz, H. Huang, F. Ford, J. Toscano, Photochemical rearrangements of diazirines and thermal rearrangements of carbenes, Pure Appl. Chem. 69 (4) (1997) 803–808.
[14] X.L. Peng, A. Migani, Q.S. Li, Z.S. Li, L. Blancafort, Theoretical study of non-Hammett vs. Hammett behaviour in the thermolysis and photolysis of arylchlorodiazirines, Phys. Chem. Chem. Phys. 20 (2) (2018) 1181–1188.
[15] M. Hashimoto, Y. Hatanaka, Recent progress in diazirine-based photoaffinity labeling, Eur. J. Org. Chem. 2008 (15) (2008) 2513–2523.
[16] J.R. Hill, A.A.B. Robertson, Fishing for drug targets: a focus on diazirine photoaffinity probe synthesis, J. Med. Chem. 61 (16) (2018) 6945–6963.
[17] S.M. Korneev, Valence isomerization between diazo compounds and diazirines, Eur. J. Org. Chem. 2011 (31) (2011) 6153–6175.
[18] K. Sakurai, T. Yasui, S. Mizuno, Comparative analysis of the reactivity of diazirine-based photoaffinity probes toward a carbohydrate-binding protein, Asian J. Org. Chem. 4 (8) (2015) 724–728.
[19] A. Admasu, A.D. Gudmundsdóttir, M.S. Platz, D.S. Watt, S. Kwiatkowski, P.J. Crocker, A laser flash photolysis study of p-tolyl (trifluoromethyl) carbene, J. Chem. Soc. Perkin Trans. 2 (5) (1998) 1093–1100.
[20] Y. Zhang, G. Burdzinski, J. Kubicki, M.S. Platz, Direct observation of carbene and diazo formation from aryldiazirines by ultrafast infrared spectroscopy, J. Am. Chem. Soc. 130 (48) (2008) 16134–16135.
[21] G.W. Preston, A.J. Wilson, Photo-induced covalent cross-linking for the analysis of biomolecular interactions, Chem. Soc. Rev. 42 (8) (2013) 3289–3301.
[22] N. Kanoh, T. Nakamura, K. Honda, H. Yamakoshi, Y. Iwabuchi, H. Osada, Distribution of photo-cross-linked products from 3-aryl-3-trifluoromethyldiazirines and alcohols, Tetrahedron 64 (24) (2008) 5692–5698.
[23] T. Akasaka, M.T.H. Liu, Y. Niino, Y. Maeda, T. Wakahara, M. Okamura, K. Kobayashi, S. Nagase, Photolysis of diazirines in the presence of C60: a chemical probe for carbene/diazomethane partitioning, J. Am. Chem. Soc. 122 (29) (2000) 7134–7135.
[24] A.B. Kumar, J.D. Tipton, R. Manetsch, 3-Trifluoromethyl-3-aryldiazirine photolabels with enhanced ambient light stability, Chem. Commun. 52 (13) (2016) 2729–2732.
[25] R. Bonneau, M.T.H. Liu, Quantum yield of formation of diazo compounds from the photolysis of diazirines, J. Am. Chem. Soc. 118 (30) (1996) 7229–7230.
[26] R. Kupfer, M.D. Poliks, U.H. Brinker, Carbene rearrangements. 43. Carbenes in constrained systems. 2. First carbene reactions within zeolites: solid-state photolysis of adamantane-2-spiro-3′-diazirine, Journal of the American Chemical Society 116 (16) (1994) 7393–7398.
[27] M. Nassal, 4-(1-Azi-2, 2, 2-trifluoroethyl) benzoic acid, a highly photolabile carbene generating label readily fixable to biochemical agents, Liebigs Annalen der Chemie 1983 (9) (1983) 1510–1523.
[28] R.A.G. Smith, J.R. Knowles, The preparation and photolysis of 3-aryl-3H-diazirines, J. Chem. Soc. Perkin Trans. 2 (7) (1975) 686–694.
[29] M.B.S. Mota, N. Rosenbach Jr., C.J.A. Mota, Theoretical studies of the insertion of carbenes in the zeolite framework: modification of the acidity and creation of chiral sites, J. Braz. Chem. Soc. 25 (2014) 1021–1028.
[30] A. Blencowe, N. Caiulo, K. Cosstick, W. Fagour, P. Heath, W. Hayes, Synthesis of hyperbranched poly(aryl ether)s via carbene insertion processes, Macromolecules 40 (4) (2007) 939–949.
[31] S. Xie, S. Manuguri, G. Proietti, J. Romson, Y. Fu, A.K. Inge, B. Wu, Y. Zhang, D. Häll, O. Ramström, M. Yan, Design and synthesis of theranostic antibiotic nanodrugs that display enhanced antibacterial activity and luminescence, Proc. Natl. Acad. Sci. 114 (32) (2017) 8464–8469.
[32] C. Hansch, A. Leo, R.W. Taft, A survey of Hammett substituent constants and resonance and field parameters, Chem. Rev. 91 (2) (1991) 165–195.
[33] V. Balachandran, V. Karpagam, G. Santhi, B. Revathi, G. Ilango, M. Kavimani, Conformational stability, vibrational (FT-IR and FT-Raman) spectra and computational

analysis of m-trifluoromethyl benzoic acid, Spectrochim. Acta A Mol. Biomol. Spectrosc. 137 (2015) 165–175.
[34] A. Gambi, M. Winnewisser, J.J. Christiansen, The infrared spectrum of diazirine: rovibrational analysis of the $\nu 3$ fundamental, J. Mol. Spectrosc. 98 (2) (1983) 413–424.
[35] V. Balachandran, A. Nataraj, T. Karthick, Molecular structure, spectroscopic (FT-IR, FT-Raman) studies and first-order molecular hyperpolarizabilities, HOMO–LUMO, NBO analysis of 2-hydroxy-p-toluic acid, Spectrochim. Acta A Mol. Biomol. Spectrosc. 104 (2013) 114–129.
[36] A. Blencowe, W. Fagour, C. Blencowe, K. Cosstick, W. Hayes, Synthesis of hyperbranched poly (aryl amine) s via a carbene insertion approach, Org. Biomol. Chem. 6 (13) (2008) 2327–2333.
[37] R. Cataliotti, A. Poletti, G. Paliani, A. Foffani, Infrared spectrum and vibrational assignment of diazocyclopentadiene-h4 and-d4, Z. Naturforsch. B 27 (8) (1972) 875–878.
[38] S.A. Brandán, F. Márquez López, M. Montejo, J.J. López González, A. Ben Altabef, Theoretical and experimental vibrational spectrum study of 4-hydroxybenzoic acid as monomer and dimer, Spectrochim. Acta A Mol. Biomol. Spectrosc. 75 (5) (2010) 1422–1434.
[39] J. Dubois, F.R. van de Voort, J. Sedman, A.A. Ismail, H.R. Ramaswamy, Quantitative Fourier transform infrared analysis for anisidine value and aldehydes in thermally stressed oils, J. Am. Oil Chem. Soc. 73 (6) (1996) 787–794.
[40] R. Amorati, M.C. Foti, L. Valgimigli, Antioxidant activity of essential oils, J. Agric. Food Chem. 61 (46) (2013) 10835–10847.
[41] Büchner-Curtius-Schlotterbeck Reaction, Comprehensive Organic Name Reactions and Reagents2010 567–569.
[42] H. Yang, B. Martin, B. Schenkel, On-demand generation and consumption of diazomethane in multistep continuous flow systems, Org. Process Res. Dev. 22 (4) (2018) 446–456.
[43] G. Burdzinski, M.S. Platz, Ultrafast kinetics of carbene reactions, in: R.A. Moss, M.P. Doyle (Eds.),Contemporary Carbene Chemistry, 2013.
[44] R. Hommelsheim, Y. Guo, Z. Yang, C. Empel, R.M. Koenigs, Blue-light-induced carbene-transfer reactions of diazoalkanes, Angew. Chem. Int. Ed. 58 (4) (2019) 1203–1207.
[45] H.S. Nanda, A.H. Shah, G. Wicaksono, O. Pokholenko, F. Gao, I. Djordjevic, T.W.J. Steele, Nonthrombogenic hydrogel coatings with carbene-cross-linking bioadhesives, Biomacromolecules 19 (5) (2018) 1425–1434.
[46] A.H. Shah, I. Djordjevic, T.W.J. Steele, Tertiary blends of PAMAM/PEG/PEG tissue bioadhesives, J. Mech. Behav. Biomed. Mater. 101 (2020) 103405.
[47] G. Wicaksono, I. Djordjevic, A.H. Shah, T.W.J. Steele, Photorheology of bioadhesive dendrimer polycaprolactone composites, Polym. Test. 80 (2019) 106099.
[48] M. Singh, C.S. Yin, S.J. Page, Y. Liu, G. Wicaksono, R. Pujar, S.K. Choudhary, G.U. Kulkarni, J. Chen, J.V. Hanna, R.D. Webster, T.W.J. Steele, Synergistic voltaglue adhesive mechanisms with alternating electric fields, Chem. Mater. 32 (6) (2020) 2440–2449.
[49] F. Gao, I. Djordjevic, O. Pokholenko, H. Zhang, J. Zhang, T. Steele, On-demand bioadhesive dendrimers with reduced cytotoxicity, Molecules 23 (4) (2018) 796.
[50] M. You, L. Liu, W. Zhang, The covalently bound diazo group as an infrared probe for hydrogen bonding environments, Phys. Chem. Chem. Phys. 19 (29) (2017) 19420–19426.
[51] Z. Xiong, T. Gu, X. Wang, Self-assembled multilayer films of sulfonated graphene and polystyrene-based diazonium salt as photo-cross-linkable supercapacitor electrodes, Langmuir 30 (2) (2014) 522–532.
[52] M. Pandurangappa, T. Ramakrishnappa, R.G. Compton, Functionalization of glassy carbon spheres by ball milling of aryl diazonium salts, Carbon 47 (9) (2009) 2186–2193.
[53] C. Mangeney, Z. Qin, S.A. Dahoumane, A. Adenier, F. Herbst, J.-P. Boudou, J. Pinson, M.M. Chehimi, Electroless ultrasonic functionalization of diamond nanoparticles using aryl diazonium salts, Diam. Relat. Mater. 17 (11) (2008) 1881–1887.
[54] S.I. Ivlev, A.J. Karttunen, M.R. Buchner, M. Conrad, R.V. Ostvald, F. Kraus, Synthesis and characterization of barium hexafluoridoosmates, Crystals 8 (1) (2018) 11.
[55] B. Musio, E. Gala, S.V. Ley, Real-time spectroscopic analysis enabling quantitative and safe consumption of fluoroform during nucleophilic trifluoromethylation in flow, ACS Sustain. Chem. Eng. 6 (1) (2018) 1489–1495.